Memoirs of the College of Science, University of Kyoto, Series A,
Vol. XXX, No. 2, Article 4, 1962.

ATMOSPHERIC MODELS OF WHITE DWARFS

BY

Akira UESUGI

(Received May 4, 1962)

ABSTRACT

Model atmospheres with high surface gravity ($\log g=8$ and 9) are computed. The adopted values of effective temperature are 10,700, 15,000 and 20,000°K, respectively. The normal abundance ratio of hydrogen to helium ($N_H : N_{He}=85:15$) is assumed. These models have higher electron pressure and opacity compared with main-sequence models.

The H_γ and H_δ profiles are computed based upon these models. The effect of wing overlapping is serious, since the wings of these lines extend more than 100 Å from each line center. The ratio, $W(H_\delta)/W(H_\gamma)$, is small and agrees with the observed value. $U-V\sim\theta_e$ relation is also computed. The effective temperature derived from this relation is lower than that in Greenstein's temperature scale. Comparisons of Balmer line profiles with observed ones are done by means of this temperature scale. It is found that the computed line absorption is too small compared with the observed one.

Correction to the temperature distribution-law for the constancy of net flux $F(\tau)$ throughout the atmosphere is applied to the models with $T_e=10{,}700°K$ with the aid of Swihart's method. The corrected surface temperature becomes much lower, and $\frac{\Delta F(\tau)}{F}$ is less than 1 per cent. For our corrected model, the computed profiles of Balmer absorption lines agree fairly well with the observed ones.

1. Introduction

Since Strömgren (1) analyzed solar spectra with his model solar atmosphere, the method of model atmosphere has been keeping its great advantage in "*Fein-Analyse*" of the stellar spectra, especially for the early type main-sequence stars. Extensive references concerning early-type model atmospheres are found in Aller's article (2).

The purpose to construct a model atmosphere is, in short, to know the physical states in a real stellar atmosphere. Many model atmospheres have been constructed by various authors. Among them, a set of models computed by de Jager and Neven (3) is worth noticing for its variety in the atmospheric parameters. However, the high surface gravity stars are excluded from this set.

Model atmospheres of the white dwarf stars are computed by several authors: Miyamoto (4) constructed pure hydrogen model for Sirius B, and pointed out

that owing to the pressure effect which reduces the ionization of the atoms, the apparent spectral type of the white dwarf corresponds to a higher effective temperature star than that of the ordinary scale for the main-sequence. Schatzman (5) discussed the distribution of the elements in the gravitational field and showed that the heavy elements have little concentration in the outer envelope of the white dwarfs. He also computed pure hydrogen model atmospheres for 40 Eri B and for van Maanen 2. According to him, the effective temperature of the white dwarf is higher than that of the main sequence star with the same color temperature, because the continuous spectrum of white dwarf is depressed by the broadened Balmer lines. Grenchik (6) also constructed a pure hydrogen model atmosphere for 40 Eri B, and computed H_γ-profile with the use of Kolb's theory. Couteau (7) presented the high temperature models that may be suitable for explaining the disappearance of absorption lines in some white dwarf stars. In this paper we compute a set of model atmospheres with high surface gravity, and discuss the temperature scale for the white dwarfs and their Balmer line spectra.

First of all, we have to decide the parameters which specify the model atmospheres. From the mass-radius relation for the degenerate stars (see, Chandrasekhar (8)) we have $7 \lesssim \log g \lesssim 9$ for $-0.66 < \log (M/M_\odot) < 0.1$. On the other hand, for the star whose mass is known, we can obtain the value of $\log g$ assuming their effective temperature. For 40 Eri B, $\log (M/M_\odot) = -0.35$, then, with assumed $T_e = 13{,}500\,^\circ$K we have $\log g = 7.68$ (Kuiper (9)). Also for Sirius B, $\log (M/M_\odot) = -0.01$, and $T_e = 12{,}500\,^\circ$K, then $\log g = 8.11$ (Miyamoto (4)).

Lynds (10) used the H_γ- and H_δ-profiles to obtain the surface gravity of the white dwarf. He assumed that the same relation between effective temperature and $B-V$ color index holds both for the main sequence and for the white dwarf stars, and compared Verweij's theoretical profile of the H_γ line with the observed one. Thus, for 13 white dwarfs which have hydrogen lines, he estimated the value of $\log g$ to be 6.8~7.5.

Greenstein (11) discussed the temperature scale for the white dwarfs. He computed $U-V$ color and H_γ equivalent width with the theoretical models and illustrated a diagram of $U-V$ color *versus* effective temperature. If $U-V$ color and H_γ equivalent width are observed with a white dwarf, the corresponding effective temperature can be known from his theoretical diagram. Greenstein found for the majority of the white dwarfs with known color indices, the effective temperature, θ_e, to be $0.1 \lesssim \theta_e \lesssim 0.7$.

Here, we take $T_e = 10{,}700$, 15,000 and 20,000 °K, and $\log g = 8.0$ and 9.0 as the parameters of the model atmosphere, and expect that such groups of models

would cover some of the observed white dwarfs. In Table 1, we listed the combinations of these parameters for 6 models.

Table 1. The parameters of model atmospheres.

Model	T_e°K	θ_e	log g
181	10,700	0.471	8.00
191	10,700	0.471	9.00
158	15,000	0.336	8.00
159	15,000	0.336	9.00
281	20,000	0.252	8.00
291	20,000	0.252	9.00

It is generally accepted that white dwarf is in the final stage of stellar evolution and its chemical composition differs from normal stars. Indeed, observations show that the spectra of some white dwarfs are quite different from those of the main sequence stars (Kuiper (**9**), Luyten (**12**) and Greenstein (**11**, **13**). There exist various kinds of white dwarf stars; as continuous spectra, helium lines only and some unidentified lines without any hydrogen lines, and so on. Weidemann (**14**) studied the spectra of van Maanen 2, one of well-known but peculiar object, and concluded that it is really underabundant in hydrogen content and even in metal contents, compared with main-sequence stars. However, among white dwarfs whose spectra are so far as available, we find a considerable number of the so-called DA type stars that are classified as having strong Balmer absorption lines. It seems that this fact does not exclude the existence of white dwarfs with normal, or hydrogen rich, chemical abundance.

Although we know little about accurate chemical composition in the atmosphere of white dwarf, it is quite interest to study the model atmosphere with normal composition. In conformity with our earlier program on the early-type main-sequence stars (Saito (**15**, **16**), and Saito and Uesugi (**17**)), here we shall construct model atmospheres of the white dwarf with the same opacity table (**18**), and discuss the features of our models and of DA type white dwarfs.

2. Model atmospheres

When constructing a model atmosphere, one of general assumptions is that the plane-parallel atmosphere is in mechanical and radiative equilibrium whose physical properties depend only on the geometrical depth z measured downward from the stellar surface.

The condition of radiative equilibrium is satisfied when an atmosphere has neither source of energy nor sink at all. This condition can be written, if energy

flows through radiative process only, as

$$\int_0^\infty \kappa_\nu(z)\, B_\nu(z)\, d\nu = \int_0^\infty \kappa_\nu(z)\, J_\nu(z)\, d\nu\,, \tag{1}$$

at the depth z, or, equivalently,

$$\frac{d}{dz}\int_0^\infty F_\nu(z)\, d\nu = 0\,, \tag{2}$$

throughout the atmosphere. Here, $\kappa_\nu(z)$ denotes the monochromatic absorption coefficient per gram of stellar matter, $B_\nu(z)$, the Planck-function, $J_\nu(z)$, the mean intensity, $F_\nu(z)$, the outward flux, for ν-radiation, respectively (cf. Unsöld (**19**)).

When the atmosphere is gray, i. e., $\kappa_\nu(z)$ is independent of ν and equals to $\bar{\kappa}(z)$, and if it is in radiative equilibrium, we have an expression for the local temperature $T(\bar{\tau})$ at the optical depth $\bar{\tau}$ as

$$T^4(\bar{\tau}) = \frac{3}{4}\, T_e^4\left\{\bar{\tau}+q(\bar{\tau})\right\}, \tag{3}$$

where T_e is the effective temperature of the star and the exact form of the function $q(\bar{\tau})$ is given by Mark (**20**). The optical depth, $\bar{\tau}$, is defined as

$$\bar{\tau}(z) = \int_0^z \bar{\kappa}(z)\, \rho(z)\, dz\,, \tag{4}$$

where $\rho(z)$ denotes the density of the atmosphere.

However, in a non-gray atmosphere where $\kappa_\nu(z)$ varies with ν, we have no such an explicit relation as Eq. (3). Hence we construct a non-gray model atmosphere with the use of this gray temperature law, keeping in mind that the result obtained is only an approximation.

As far as we adopt the gray-law (3), instead of the non-gray one, we must use some sort of mean absorption coefficient $\kappa(z)$ which corresponds to the gray absorption coefficient $\bar{\kappa}(z)$. There are three types of mean opacity (cf. Kourganoff (**21**)); Rosseland mean, Planck mean and Chandrasekhar mean. Discussion on the choice of mean opacity has been done by several authors (Unsöld (**22**), Michard (**23**), ten Bruggencate (**24**) and Saito (**25**)). The principal point of this discussion consists in what type of mean would give a better approximation than the others. Hence so far as we are intending to correct the temperature law, after having a model atmosphere in the first approximation, a particular choice of mean opactiy seems less important. Here, as noted, we use the Rosseland mean.

Now, following Labs (**26**), we adopt the following expression for the function $q(\tau)$ given by

$$q(\tau) = 0.7104 - 0.1331 \exp\left[-3.4488\tau\right]. \tag{5}$$

Since the initial temperature law is only an approximation, exact expression to

$q(\tau)$ has no significance and it is sufficient to use an expression such as Eq. (5), which is much simpler than the exact $q(\tau)$.

The equation of hydrostatic equilibrium is written in the form

$$\frac{dP(z)}{dz} = \rho(z)\, g\,, \tag{6}$$

where g denotes the surface gravity and $P(z)$, total pressure which is the sum of the gas pressure, $P_g(z)$, and the radiation pressure. We define the optical depth τ as

$$\tau = \int_0^z \kappa(z)\, \rho(z)\, dz\,, \tag{7}$$

where $\kappa(z)$ is the Rosseland mean opacity. Then from Eq. (6) we have

$$\frac{dP(\tau)}{d\tau} = \frac{g}{\kappa(\tau)}\,. \tag{8}$$

Now, negative gravity, g', due to radiation pressure is expressed as

$$g' = \kappa \frac{\sigma}{c} T_e^4\,, \tag{9}$$

(cf. Unsöld (**19**)). When we take 2×10^4 °K for T_e, and substitute the numerical values of the Stefan-Boltzmann constant σ and the light velocity c, we obtain $g'\sim3\times10^2\kappa$. Since κ is 10^3 at most, $g'\lesssim3\times10^5$ which is negligible compared with our adopted value g, 10^8 and 10^9. Thus, we shall hereafter drop the factor of radiation pressure in $P(z)$. Then, Eq. (8) is written as

$$\frac{dP_g(\tau)}{d\tau} = \frac{g}{\kappa(\tau)}\,. \tag{10}$$

$P_g(\tau)$ and $\kappa(\tau)$ are functions of electron pressure, $P_e(\tau)$, and temperature, $T(\tau)$. Since $T(\tau)$ is related to τ through Eqs. (3) and (5), we can integrate Eq. (10) and obtain the values of $P_g(\tau)$, $P_e(\tau)$ and $\kappa(\tau)$, for each level τ, successively. The results are given in Tables 2·1~2·6.

In these tables, the first column contains optical depth τ. The second and third columns give the reciprocal temperature, θ $(=5040/T)$, and temperature, T (°K), respectively. The logarithms of gas- and electron-pressure and those of mean opacity κ are found in the fourth, fifth and sixth columns, respectively. The last two columns contain the fraction of atoms in neutral stage, for hydrygen, $y_{\rm H}$, and also for helium, $y_{\rm He}$.

The effect of high surface gravity is obviously seen in progressions of both gas- and electron-pressure. Comparing our models with those of the main-sequence stars, we find that $\log P_g$, at a definite optical depth, is roughly

Table 2·1. Model 181.
T_e=10,700°K log g=8.0

τ	θ	T	log P_g	log P_e	log κ	log y_H	log y_{He}
0.001	0.580	8.69(3)	4.295	2.851	0.792	$\bar{1}$.982	0.000
5	579	8.71	860	3.153	941	990	
0.01	577	8.73	5.095	287	1.019	992	
2	574	8.79	323	430	111	994	
3	570	8.84	451	520	173	994	
4	567	8.89	540	589	220	995	
6	561	8.98	660	694	290	995	
8	555	9.07	743	781	351	995	
0.1	550	9.16	804	852	406	995	
2	528	9.55	978	4.111	606	993	
3	511	9.87	6.066	286	741	992	
4	497	1.02(4)	123	423	843	990	
5	485	1.04	163	533	936	988	
6	475	1.06	194	629	2.013	986	
8	457	1.10	238	785	136	982	
1.0	443	1.14	270	910	240	977	
1.4	420	1.20	312	5.104	396	966	
2.0	394	1.28	352	313	569	947	
3.0	365	1.38	393	545	752	908	
4.0	344	1.47	419	695	864	861	
5.0	327	1.54	440	804	935	811	
6.0	314	1.60	457	884	977	755	
8.0	295	1.72	486	992	3.021	639	$\bar{1}$.999
10.0	280	1.80	512	6.054	026	519	997
14.0	258	1.95	560	159	017	321	990
20.0	237	2.13	626	255	2.992	082	968

Table 2·2. Model 191.
T_e=10,700°K log g=9.0

τ	θ	T	log P_g	log P_e	log κ	log y_H	log y_{He}
0.001	0.580	8.69(3)	5.108	3.268	0.997	$\bar{1}$.973	0.000
5	579	8.71	649	557	1.175	996	
0.01	577	8.73	873	684	259	997	
2	574	8.79	6.095	802	338	997	
3	570	8.84	221	911	418	998	
4	567	8.89	307	981	467	998	
6	561	8.98	424	4.084	543	998	
8	555	9.07	503	166	606	998	
0.1	550	9.16	563	236	656	998	
2	528	9.55	736	494	844	997	
3	511	9.87	831	675	976	997	
4	497	1.02(4)	888	814	2.073	996	
5	485	1.04	929	925	153	995	
6	475	1.06	961	5.022	223	994	
8	457	1.10	7.010	182	335	993	
1.0	443	1.14	043	313	429	991	
1.4	420	1.20	091	513	577	987	
2.0	394	1.28	136	736	736	979	
3.0	365	1.38	180	991	925	965	
4.0	344	1.47	209	6.161	3.069	947	
5.0	327	1.54	229	283	159	928	
6.0	314	1.60	245	385	233	907	
8.0	295	1.72	269	531	330	862	
10.0	280	1.80	289	639	388	816	
14.0	258	1.95	322	771	442	716	
20.0	237	2.13	363	895	493	573	

Table 2·3. Model 158.
T_e=15,000°K log g=8.0

τ	θ	T	log P_g	log P_e	log κ	log y_H	log y_{He}
0.001	0.414	1.22(4)	3.756	3.377	1.503	$\bar{1}$.191	0.000
5	413	1.22	4.154	727	777	453	
0.01	412	1.23	333	881	883	544	
2	409	1.23	520	4.040	983	618	
3	407	1.24	632	134	2.037	650	
4	405	1.25	713	203	081	667	
6	400	1.26	827	311	141	688	
8	396	1.27	908	388	181	693	
0.1	393	1.28	972	447	212	692	
2	377	1.34	5.167	661	328	668	
3	364	1.38	280	796	400	631	
4	354	1.42	359	892	439	588	
5	346	1.46	421	970	471	549	
6	339	1.49	472	5.047	500	511	$\bar{1}$.999
8	326	1.55	554	134	528	433	999
1.0	316	1.60	618	214	546	363	998
1.4	300	1.68	723	340	556	240	996
2.0	281	1.79	842	476	562	086	989
3.0	260	1.94	987	635	562	$\bar{2}$.893	971
4.0	245	2.06	6.093	749	574	747	941
5.0	234	2.16	177	839	586	635	901
6.0	224	2.25	245	912	597	543	853
8.0	210	2.40	353	6.027	616	400	743
10.0	200	2.53	436	116	631	290	626
14.0	184	2.73	561	249	654	132	410
20.0	169	2.98	692	387	687	$\bar{3}$.974	150

Table 2·4. Model 159.
T_e=15,000°K log g=9.0

τ	θ	T	log P_g	log P_e	log κ	log y_H	log y_{He}
0.001	0.414	1.22(4)	4.328	3.870	1.880	$\bar{1}$.562	0.000
5	413	1.22	782	4.222	2.083	743	
0.01	412	1.23	993	386	156	798	
2	409	1.23	5.210	533	232	873	
3	407	1.24	337	629	280	855	
4	405	1.25	428	699	314	864	
6	400	1.26	555	807	371	874	
8	396	1.27	644	885	409	877	
0.1	393	1.28	712	950	443	878	
2	377	1.34	916	5.172	575	869	
3	364	1.38	6.027	321	663	854	
4	354	1.42	102	430	729	836	
5	346	1.46	159	514	778	818	
6	339	1.49	305	589	825	800	
8	326	1.55	275	696	880	760	
1.0	316	1.60	329	786	926	723	
1.4	300	1.68	411	918	985	647	999
2.0	281	1.79	502	6.050	3.028	535	997
3.0	260	1.94	611	201	061	376	992
4.0	245	2.06	694	303	074	243	983
5.0	234	2.16	762	386	085	137	969
6.0	224	2.25	819	455	087	050	953
8.0	210	2.40	914	562	102	$\bar{2}$.909	908
10.0	200	2.53	990	648	118	801	853
14.0	184	2.73	7.106	779	138	649	733
20.0	169	2.98	229	912	177	489	550

Table 2·5. Model 281.
T_e=20,000°K log g=8.0

τ	θ	T	log P_g	log P_e	log κ	log y_H	log y_{He}
0.001	0.311	1.62(4)	4.086	3.753	1.182	$\bar{3}$.920	$\bar{1}$.920
5	310	1.63	459	4.121	517	$\bar{2}$.270	962
0.01	309	1.63	619	278	655	407	972
2	307	1.64	780	436	793	531	978
3	305	1.65	875	531	870	592	980
4	303	1.66	943	600	923	630	981
6	300	1.68	5.040	695	992	669	981
8	297	1.70	111	764	2.035	685	980
0.1	294	1.71	167	819	066	692	979
2	283	1.78	350	5.008	154	674	971
3	273	1.84	464	121	192	629	960
4	266	1.90	549	206	216	583	947
5	259	1.94	616	277	235	542	933
6	254	1.99	672	336	256	505	917
8	245	2.06	762	428	283	432	881
1.0	237	2.13	832	500	301	366	839
1.4	225	2.24	941	615	332	261	750
2.0	211	2.39	6.059	740	356	133	606
3.0	195	2.58	196	884	386	$\bar{3}$.978	381
4.0	184	2.74	296	985	402	861	187
5.0	175	2.88	374	6.066	419	774	030
6.0	168	3.00	438	134	434	702	$\bar{2}$.895
8.0	158	3.20	538	238	461	595	686
10.0	150	3.37	616	316	479	508	520
14.0	138	3.64	733	433	509	385	278
20.0	127	3.97	857	557	546	260	032

Table 2·6. Model 291.
T_e=20,000°K log g=9.0

τ	θ	T	log P_g	log P_e	log κ	log y_H	log y_{He}
0.001	0.311	1.62(4)	4.616	4.274	1.664	$\bar{2}$.433	$\bar{1}$.975
5	310	1.63	983	631	997	762	988
0.01	309	1.63	5.142	785	2.132	890	991
2	307	1.64	305	941	262	$\bar{1}$.004	993
3	305	1.65	402	5.034	332	059	994
4	303	1.66	472	102	378	093	994
6	300	1.68	573	202	443	133	994
8	297	1.70	636	272	484	149	994
0.1	294	1.71	704	329	515	156	994
2	283	1.78	891	520	606	143	991
3	273	1.84	6.006	638	649	105	988
4	266	1.90	090	724	678	065	983
5	259	1.94	157	797	704	029	979
6	254	1.99	212	853	721	$\bar{2}$.991	973
8	245	2.06	300	947	750	925	960
1.0	237	2.13	370	6.021	771	865	945
1.4	225	2.24	476	133	800	761	908
2.0	211	2.39	593	259	830	638	839
3.0	195	2.58	726	401	869	485	708
4.0	184	2.74	822	503	892	372	574
5.0	175	2.88	897	581	911	283	450
6.0	168	3.00	955	645	924	209	337
8.0	158	3.20	7.057	748	955	101	153
10.0	150	3.37	133	828	976	016	000
14.0	138	3.64	246	940	$\bar{3}$.014	$\bar{3}$.889	$\bar{2}$.767
20.0	127	3.97	366	7.061	050	763	527

proportional to $\log g$. Also, the effect of high value of gravity is seen in y_{H} and y_{He}. Ionization of hydrogen is not so highly proceeding even in the case of our models with $T_e=15{,}000\,^{\circ}\mathrm{K}$, though they should be assigned to B5 type star on the usual temperature scale. This is the fact which simply reflects the fashion of ionization. In Saha's equation, temperature and electron-pressure are the opponent factors to each other; the higher the temperature and the lower the electron-pressure, the higher the ionization degree. Therefore, even if the spectral features are similar in white dwarf and in main-sequence stars, this similarity does not simply mean the similarity of temperature.

As we have already had the relevant physical quantities in our model atmospheres, we can compute the radiative flux of these models.

Since the scattering by free electron is negligible compared with atomic absorption, the monochromatic absorption coefficient is computed as:

$$\kappa_\nu = \frac{1}{m_{\mathrm{H}}\mu}\left[\nu_{\mathrm{H}} m_{\mathrm{H}}\left\{\kappa_\nu(\mathrm{H})+\kappa_\nu(\mathrm{H}^-)\right\}+\nu_{\mathrm{He}} m_{\mathrm{He}}\left\{\kappa_\nu(\mathrm{He})+\kappa_\nu(\mathrm{He}^+)\right\}\right](1-e^{-h\nu/kT}), \quad (11)$$

where the absorption coefficient for the i-kind of element, $\kappa_\nu(i)$, is related to the atomic absorption coefficient $k_\nu(i)$ through the relation

$$\kappa_\nu(i) = \frac{k_\nu(i)}{m_i} y_i, \quad (12)$$

and the other notations are as usual. Numerical values of $k_\nu(i)$ for H, He and He^+ are tabulated by Ueno, Saito and Jugaku (**27**).

Defining the monochromatic optical depth as

$$\tau_\nu = \int_0^\tau \frac{\kappa_\nu}{\kappa} d\tau, \quad (13)$$

we have following expression (cf. Unsöld (**19**)) for the monochromatic flux $F_\nu(\tau_\nu)$ at depth τ_ν,

$$\begin{aligned} F_\nu(\tau_\nu) &= \mathcal{D}_{\tau_\nu}\left\{B_\nu(t_\nu)\right\} \\ &\equiv 2\int_{\tau_\nu}^{\infty} B_\nu(t_\nu)\, E_2(t_\nu-\tau_\nu)\, dt_\nu - 2\int_0^{\tau_\nu} B_\nu(t_\nu)\, E_2(\tau_\nu-t_\nu)\, dt_\nu . \end{aligned} \quad (14)$$

In Eq. (14), we assumed that the source function is equal to the Planck function, $B_\nu(T)$, of local temperature T at the depth τ_ν. For the emergent flux of the atmosphere, form Eq. (14), we have

$$F_\nu(0) = 2\int_0^{\infty} B_\nu(t_\nu)\, E_2(t_\nu)\, dt_\nu . \quad (15)$$

The results of the computed emergent flux for our 6 models are shown in Table 3, and illustrated in Figs. 1.1 and 1.2. In Table 3, the computed effective

Table 3. The emergent flux.

Model T_e °K log g	181 10,700 8.0	191 10,700 9.0	158 15,000 8.0	159 15,000 9.0	281 20,000 8.0	291 20,000 9.0
ν						
5.945(15)					0.00(−3)	0.00(−3)
4.617					00	00
3.288_+					03	03
3.288_-	0.26(−4)	0.27(−4)	2.30(−4)	2.32(−4)	1.18	1.17
2.932	30	31	2.38	2.41	1.10	1.09
2.576	36	36	2.51	2.50	1.06	1.04
2.220	44	45	2.69	2.72	1.04	1.03
1.865	57	60	2.97	3.04	1.04	1.03
1.509	76	83	3.37	4.47	1.04	1.03
1.153	1.05	1.16	3.79	3.88	1.00	1.00
9.875(14)	1.22	1.35	3.95	4.00	0.96	0.96
8.220_+	1.36	1.48	3.95	3.97	87	87
8.220_-	2.36	2.11	6.28	6.16	1.10	1.90
6.742	2.22	2.08	5.20	5.20	0.89	0.88
5.263	1.96	1.89	3.95	3.97	65	64
4.938	1.87	1.82	3.68	3.69	59	59
4.612	1.79	1.74	3.37	3.38	54	54
4.133	1.61	1.59	2.93	2.94	47	47
3.653_+	1.43	1.43	2.48	2.51	39	39
3.653_-	1.68	1.47	2.67	2.67	40	40
2.854	1.14	1.12	1.84	1.83	27	27
2.055	0.72	0.73	1.08	1.09	17	16
T_e^* °K	1.10(4)	1.11(4)	1.53(4)	1.53(4)	2.02(4)	2.02(4)

temperature T_e^* for each model is also given, where T_e^* is defined as

$$\frac{\sigma}{\pi}\left\{T_e^*\right\}^4 = \int_0^\infty F_\nu(0)\,d\nu\,. \tag{16}$$

T_e^* is slightly greater than the originally assumed T_e. This is a quite general feature if a model atmosphere is computed with the use of Rosseland mean absorption coefficient (cf. Saito (**16**)). As far as the outermost layer of a star is concerned, the Rosseland mean absorption coefficient is a poor approximation of the true mean (Unsöld (**22**)). Furthermore, the non-grayness of the atmosphere depresses the surface temperature to a lower value than that for the gray atmosphere (Münch .(**28**)). These are the reasons why the total flux at the surface, $F(0)$, predicts rather higher value in our models.

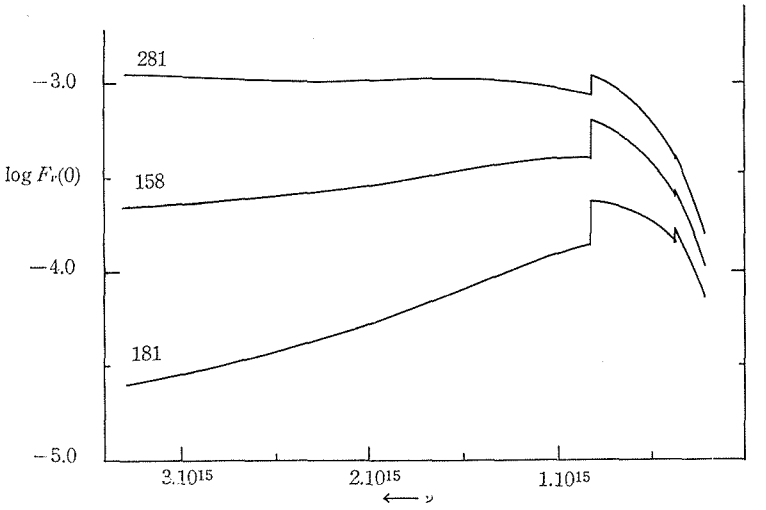

Fig. 1·1. Emergent flux for models with $\log g=8.0$.

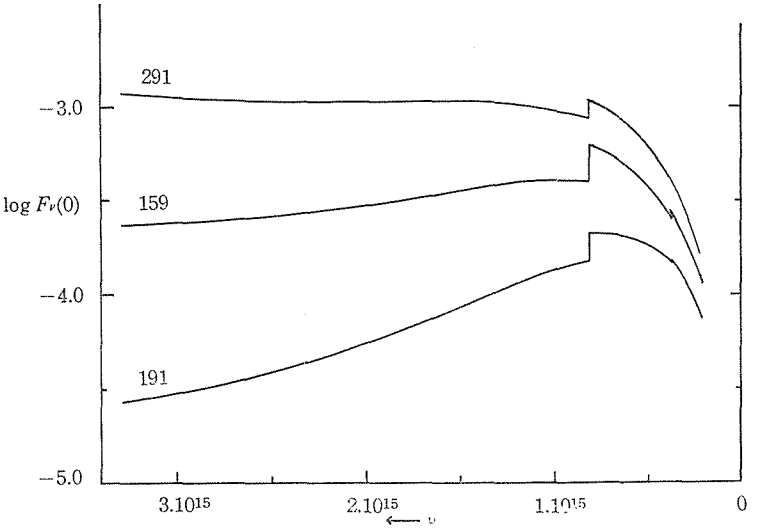

Fig. 1·2. Emergent flux for models with $\log g=9.0$.

We can also compute the Balmer jump, D, defined as:

$$D = \log \frac{F(3647_+)}{F(3647_-)}. \tag{17}$$

But when we use this formula, we must carefully deal with the flux at the red side of the Balmer limit. From Tables 2·1~2·6, we see that electron pressure is high, and hence we may expect the pronounced Stark broadening of hydrogen

lines in white dwarf spectra. To check the quantum number n of the last visible Balmer line, we have used the Inglis-Teller formula, obtaining the results as shown in Table 4. Here we have adopted the values of physical quantities at the depth where the monochromatic optical depth at λ 3647$_+$ Å is 0.6 for their characteristic values. The small value in Table 4 suggests that the higher members of Balmar series are crowded, and then continuous flux at the red side of Balmer jump is much reduced. The true emergent flux at the red side of λ 3647 Å would be smaller than the calculated one. Hence the D-value computed with the formula (17), which is also given in Table 4, is only its upper limit. The results for main-sequence model atmosphere (**16**) are also shown in the last 3 lines of Table 4. The difference in D-value is large in the lower temperature.

Table 4. The quantum number n of the last visible Balmer line, and the Balmer jump D.

Model	T_e	log g	n	D
181	10,700	8.0	9.3	0.24
191	10,700	9.0	7.9	0.15
158	15,000	8.0	8.8	0.20
159	15,000	9.0	7.5	0.19
281	20,000	8.0	8.4	0.10
291	20,000	9.0	7.2	0.10
I	10,700	4.2	17.4	0.45
II	15,500	3.8	17.0	0.18
III	20,400	3.8	16.2	0.09

The three-color photometry system by Johnson and Morgan is used in surveying white dwards. In this system, a star is characterized by two color indices; $B-V$ and $U-B$. Here, U, B, and V are expressed in magnitude which are the measure of the emergent flux in the corresponding spectral region. We write the magnitude in i-color as $m(i)$;

$$m(i) = -2.5 \log \int_0^\infty \phi_i(\lambda) F_\lambda(0) d\lambda , \tag{18}$$

where $\phi_i(\lambda)$ is the corresponding response function in Johnson-Morgan color photometry system (**29**).

We can compute $m(i)$'s numerically with our models. The color indices are then given by

$$U-B = m(U)-m(B)+c_1 , \tag{19}$$

and

$$B-V = m(B)-m(V)+c_2 , \tag{20}$$

The two constants, c_1 and c_2, should be set up so as to fit the system of the computed color indices with the observed ones. For this purpose, we computed the solar color indices with the formulae (18), (19) and (20). Here, as $F_\lambda(0)$, we have used Pettit's solar energy curve (30). Then to get solar values, $U-B=0.16$ and $B-V=0.64$ (31), we fixed two constants as

$$c_1 = -0.92 \quad \text{and} \quad c_2 = 0.99 . \tag{21}$$

The color indices computed for our models are given in Table 5. In these computations, however, we did not take into account the effect of line absorption. Therefore, these tabulated values are not so accurate as to serve for fixing the temperature scale of the white dwarfs.

Table 5. Color indices of model atmosphere.

Model	*U-B*	*B-V*	*U-V*
181	−0.69	−0.02	−0.71
191	−0.79	+0.02	−0.77
158	−0.89	−0.17	−1.06
159	−0.89	−0.16	−1.05
281	−1.12	−0.20	−1.32
291	−1.12	−0.20	−1.32

3. The Balmer absorption lines

Recently the problem of hydrogen line broadening has been received much attention both in theoretical and experimental aspects. The most conspicuous result obtained in this field is Kolb's theory, in which the hydrogen line broadening is treated as due to both electrons and ions. A concise picture of this problem from the astrophysical viewpoint is given by Aller and Jugaku (32).

The absorption coefficient of the hydrogen line at the distance $\Delta\lambda$ from its center, λ_0, is expressed as (cf. Griem, Kolb and Shen (33), and also Aller and Jugaku (34)):

$$l(\Delta\lambda) = l_{\mathrm{H}}(\Delta\lambda)\left[1+\sqrt[3]{\Delta\lambda}\, R(N, T)\right], \tag{22}$$

where $l_{\mathrm{H}}(\Delta\lambda)$ denotes the classical Holtsmark profile and the second term in the bracket represents the correction due to the effect of electronic contribution which depends on the electron density N and the temperature T. Table of $R(N, T)$ for various values of N and T are found in the above-cited references, for H_α to H_δ.*

* The author is much indebted to Dr. J. Jugaku who kindly enabled him to use the graphical representation of $R(N, T)$ in advance of its publication.

Now we obtain the total absorption coefficient per gram of stellar matter, $\kappa^{\text{total}}(\Delta\lambda)$, which is the sum of the absorption coefficient of line, $l(\Delta\lambda)$, and that of continuum, κ^c,

$$\kappa^{\text{total}}(\Delta\lambda) = l(\Delta\lambda) + \kappa^c , \tag{23}$$

at the distance $\Delta\lambda$ from the line center. Hence, defining the optical depth $t_{\Delta\lambda}$ as

$$t_{\Delta\lambda} = \int_0^\tau \frac{\kappa^{\text{total}}(\Delta\lambda)}{\kappa} d\tau , \tag{24}$$

we have the emergent flux at $\Delta\lambda$,

$$F_{\Delta\lambda}(0) = \int_0^\infty B(t_{\Delta\lambda})\, E_2(t_{\Delta\lambda})\, dt_{\Delta\lambda} . \tag{25}$$

However, as shown in the previous section, electron pressure is extremely high for these stars, and the Inglis-Teller formula predicts that even H_8 becomes invisible, so that we must take into account the overlapping effect of wings for adjacent hydrogen absorption lines. Concerning this problem, Schatzman (5) has already examined the effect of line overlapping with his models and showed that the energy distribution in the blue region is seriously distorted by this crowding effect and the tendency of calculated emergent flux agrees approximately with the observed spectra.

On the other hand, if we consider the equivalent width of the i-th Balmer line, $W(H_i)$, we find observationally that its ratio to $W(H_\gamma)$ is smaller and the decrease of $W(H_i)/W(H_\gamma)$ as i increases is steeper in white dwarfs than in main sequence stars. From this fact, we may infer that the effect of overlapping of adjacent Balmer lines is serious. Between the two adjacent absorption lines, the extended wings of each line depress the continuous flux. As the equivalent width is measured referring to nearby continuum, it becomes smaller than in the continuum free from the blending of lines. The higher the series number, the more serious this effect.

After these considerations we define the atmospheric absorption coefficient $\kappa^{\text{total}}(\lambda)$ at the wavelength λ, including both the line and continuum as,

$$\kappa^{\text{total}}(\lambda) = \kappa^c(\lambda) + \sum_i l_i(\lambda) , \tag{26}$$

where summation over the line absorption coefficient of the i-th member $l_i(\lambda)$, is extended to include all the effect of line absorption from Balmer series member. With the aid of this formula, the values of $\kappa^{\text{total}}(\lambda)$ are computed at 28 points of wavelength between $\lambda\lambda$ 4000 and 4540 Å where H_γ (λ 4340 Å), H_δ (λ 4100 Å) and the red side of H_ε (λ 3970 Å) lines are included. For H_ε and higher members,

there was not any published table of $R(N, T)$*. So, it was approximated by that for H_δ, and hence the absorption of H_ε may be somewhat underestimated. As we computed $\kappa^{\text{total}}(\lambda)$ as a function of optical depth τ, we can find the monochromatic optical depth t_λ at wavelength λ, as usual. The source function, $B(\lambda, \tau)$, which varies with λ is also computed at corresponding λ-point. The emergent flux, $F_\lambda(0)$, at λ can easily be obtained with straightforward application of Eq. (25).

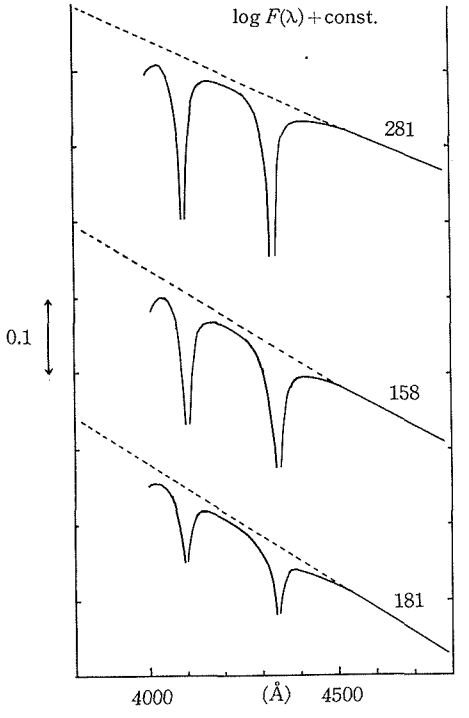

Fig. 2·1. Emergent flux in the region of H_γ and H_δ for models with $\log g=8.0$.

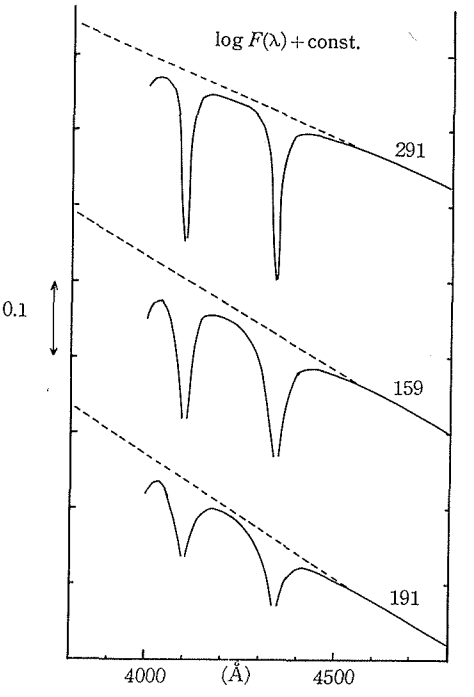

Fig. 2·2. Emergent flux in the region of H_γ and H_δ for models with $\log g=9.0$.

In Figs. 2·1 and 2·2, we show $\log F_\lambda(0)$ in the region $\lambda\lambda$ 4000~4600 Å, for our model atmospheres. The effect of wing overlapping is obvious. As shown in these figures, the line widths are enormously large and the levels of continuum at the violetward- and redward-side of each line wing are different. The line depth, R, is defined as,

* After our computational works have been completed, an approximate formula to compute the $R(N, T)$ for higher series member of Balmer lines was published by Griem (**35**), and it could not be used here.

$$R = \frac{F(\text{line})}{F(\text{cont})} . \tag{27}$$

As F(cont) varies within a line, we must regard the denominator in the above expression as a function of λ. Tentatively F(cont) is defined as follows; for a line, we draw a straight line which contacts with the wings at both sides of line center, and assume that this straight line is the continuum level. Thus F(cont) at λ is graphically interpolated, and then R is computed at each λ.

The equivalent width of a line is computed as

$$W = \int_0^\infty R d\lambda . \tag{28}$$

Interpolating again graphically the values of R for H_γ and for H_δ, we compute numerically $W(H_\gamma)$ and $W(H_\delta)$. Table 6 contains $W(H_\gamma)$ and $W(H_\delta)$ for our models. Also, the ratio, $W(H_\delta)/W(H_\gamma)$, is given. The average value of this ratio for the real DA type of white dwarfs is 0.75. We see that the coincidence between observation and computation is fairly well.

Table 6. The equivalent widths of Balmer lines.

Model	T_e °K	log g	$W(H_\gamma)$	$W(H_\delta)$	$W(H_\delta)/W(H_\gamma)$
181	10,700	8.0	18.3	14.4	0.79
191	10,700	9.0	15.8	13.5	0.86
158	15,000	8.0	16.6	13.4	0.81
159	15,000	9.0	21.6	15.5	0.72
281	20,000	8.0	9.1	7.8	0.85
291	20,000	9.0	12.8	8.8	0.69

As noted in the previous section, the line absorption has some effect on the color indices. Here we shall correct the previous color estimation including the effect of line absorption. We use also the formulae (18)～(21) in this case. $F_\lambda(0)$ is read from Figs. 2·1 and 2·2. Furthermore, the energy subtracted by the absorption lines is also taken into account. In such a manner, we obtain some knowledge about the effect of line crowding in the blue region of white dwarf spectra.

The color indices obtained above are shown in Table 7. Since B-color, and also U-color to some extent, are suppressed, the newly computed colors are somewhat different from those in Table 5. We may consider that these corrected color indices are more reliable than the previous uncorrected values. Then we take this series of color indices to predict the effective temperature of a white dwarf through color measurement.

Table 7. The color indices of model atmospheres.

Model	*U-B*	*B-V*	*U-V*
181	−0.67	+0.06	−0.61
191	−0.80	+0.09	−0.71
158	−0.87	−0.10	−0.97
159	−0.90	−0.04	−0.94
281	−1.12	−0.16	−1.28
291	−1.13	−0.14	−1.27

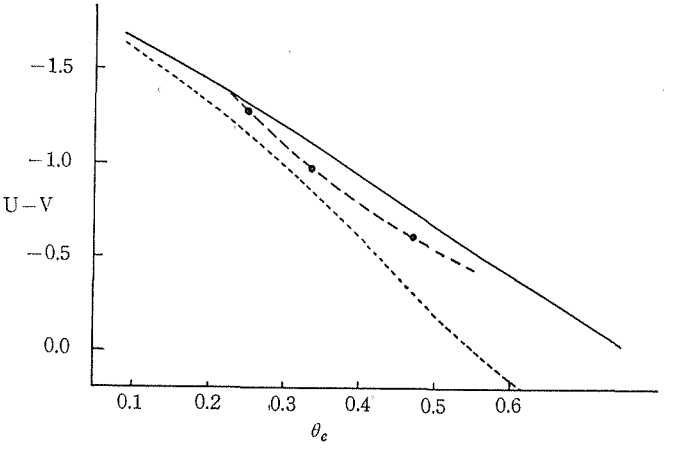

Fig. 3. *U-V versus* θ_e relation.

In Fig. 3, we plotted the $U-V$ color indices against θ_e and compared with Greenstein's results (**11**). Greenstein's computation is done in a rather approximative fashion. He took only one representative value of emergent flux in computing the colors, instead of integration, Eq. (18), in our case. He assumed that the hydrogen atom is the only source of continuous absorption. This assumption may be permitted for the star with small Balmer jump, but this is a crude assumption for the lower temperature stars. In his second approximation, he corrected colors somewhat arbitrarily. In Fig. 3, the dotted line represents Greenstein's second approximation, and the full line corresponds to the color for the stars without Balmer jump. Our results fall between these two curves. As Greenstein noted, his color-temperature relation predicts too high temperature for the DA type stars. We prefer a relation between $U-V$ and θ_e which gives lower temperature than that given by Greenstein.

There is a little difference in $U-V$ color between different $\log g$-valued model with high temperature. From a comparison of computed Blamer line

profile with observation, we rather prefer model 181 than model 191 (see later lines), and we take a set of points with $\log g=8$, in Fig. 3, for the representatives of white dwarfs. Interpolating these points (broken line), we have a $U-V\sim\theta_e$ relation.

Next, we shall compare the computed Balmer line profiles with the observed ones.

With $U-V\sim\theta_e$ relation, we can tentatively assign an effective temperature to a white dwarf. We shall pick up some white dwarfs whose effective temperatures are similar to one of our models. The computed models are divided into 3 groups with respect to their effective temperature. $U-V$ color of HZ 43 is similar to the models of the first group, $\theta_e=0.25$. 4 stars, He 3, HZ 2, W 1346 and 70° 5824, correspond to the second group with $\theta_e=0.34$. 40 Eri B and 73° 8021 may be compared with the models of $\theta_e=0.47$. In the following, some remarks on individual models are given. The observed profiles are reproduced from Greenstein's article (**13**).

The wing part of H_γ line of HZ 43 is predicted by model 291, (see Fig. 4·1). However, HZ 43 has shallow inner wing. For H_δ, the observed profiles are too shallow. This star is the bluest object among the DA type. If this star is hydrogen rich, the effective temperature should be higher than $\theta_e=0.25$.

In Figs. 4·2~4·5, we give comparisons of models 158 and 159 with 4 stars. For HZ 2, the observed profiles agree well with the computed with model 159. He 3 and W 1346 have somewhat depressed wing than the computed one. The central intensities of these two stars are smaller than that of HZ 2 and the agreement with models is not good. For 70° 5824, we cannot predict its line profiles at all. The Balmer absorption in 70° 5824 is larger than the computed. Although the color indices of these four stars are similar, the equivalent widths of H_γ are widely different. $W(H_\gamma)$ for 70° 5824, the largest among these four stars, is 35.4, while 22.7 for HZ 2. Here we might have to consider the effect of different chemical abundance among these DA type stars. Because if we change our $\log g$ to predict correct equivalent widths we have different color indices. As the predicted $W(H_\gamma)$ is only 21.6 for model 159, and this value is smaller than any of the observed ones, there may be a defect in the structure of the model.

A similar situation is found for the case of models 181 and 191. As seen in Figs. 4·6 and 4·7 in which we compare models 181 and 191 with 40 Eri B and 73° 8031, respectively, the computed profiles are entirely more shallow than the observed ones. $W(H_\gamma)$ is 31.7 for 40 Eri B and, 37.3 for 73° 8031, while 18.3 for model 181, only a half of the observed value.

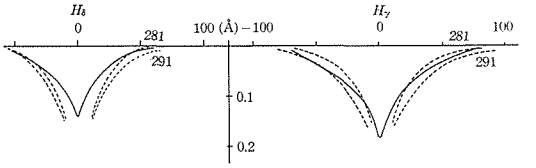

Fig. 4·1. Comparison with *HZ* 43. – – – Medel.

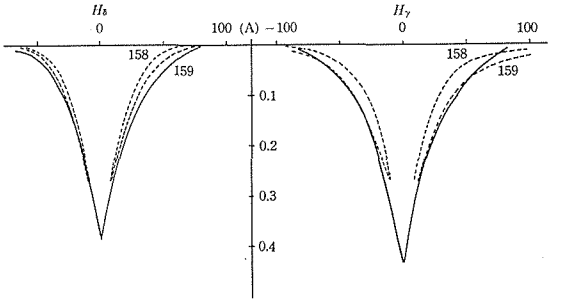

Fig. 4·2. Comparison with *HZ* 2. – – – Model.

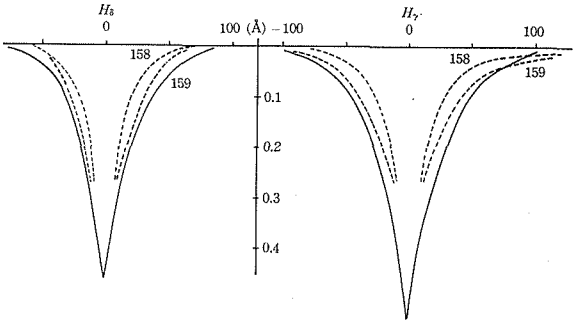

Fig. 4·3. Comparison with *He* 3 – – – Model.

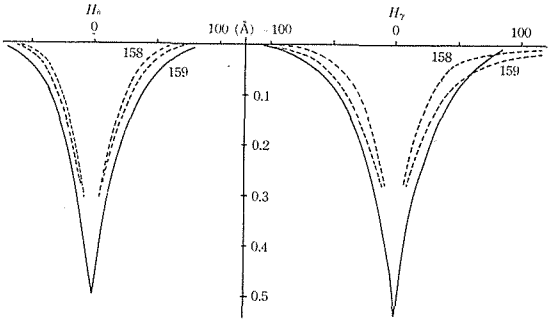

Fig. 4·4. Comparison with *W* 1346.. – – – Model.

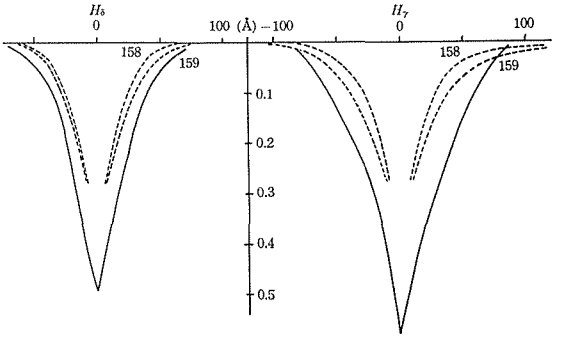

Fig. 4·5. Comparison with 70° 5824.
– – – Model.

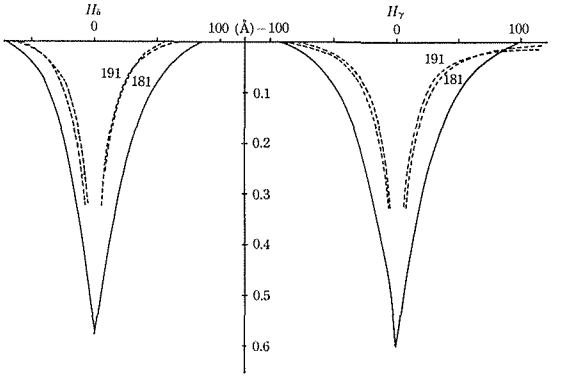

Fig. 4·6. Comparison with 40 Eri *E*.
– – – Model.

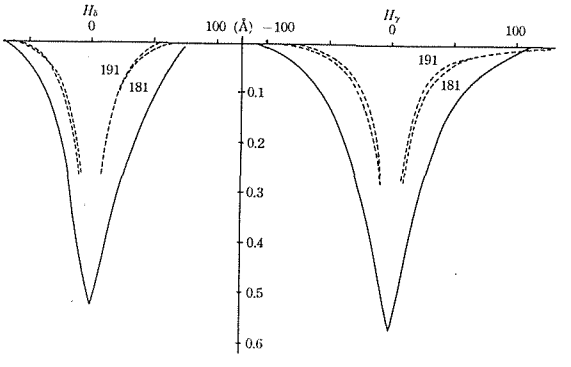

Fig. 4·7. Comparison with 73° 8031.
– – – Model.

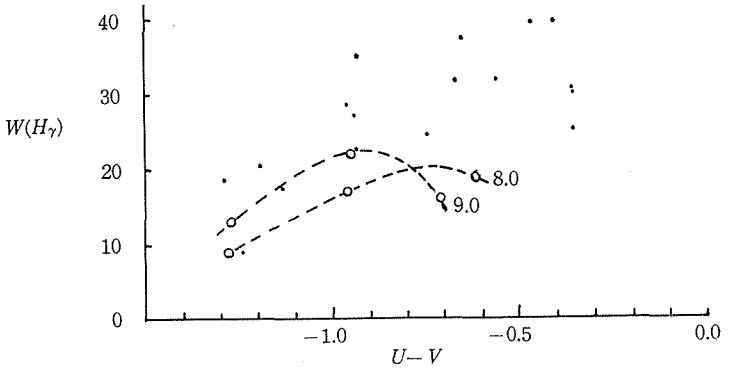

Fig. 5. $W(H_\gamma)$ *versus* U-V.
· Observed. ○ Model (log g as parameter).

In Fig. 5, we show the relation between $W(H_\gamma)$ and the $U-V$ colors for our models and for the observed white dwarfs. As we see, the models predict smaller $W(H_\gamma)$ and the discrepancy is larger in cooler stars. We assume that the observed profiles may be interpreted with models in normal abundance, and we examine some possibilities to reduce this discrepancy. First, we may have some illusions that if the surface gravity is higher, the agreement should be improved. However, so far as the low T_e models are concerned, this would not be the case. Because, as seen in Table 6, the higher the surface gravity, the larger the continuous opacity, and then the line absorption will not necessarily increase with the surface gravity. The next simple interpretation is to push down the surface temperature of the models. As shown in Table 8, the layer where the Balmer lines originate, is an outermost upper layer of the atmosphere, and if we take lower T at small τ, we have deeper absorption lines.

Table 8. τ_{eff}, the mean optical depth corresponding to $\tau_{4446+}=0.6$.

T_e °K	log g	τ_{eff}
10,700	8.0	0.69
10,700	9.0	0.55
10,700	4.2	1.49
15,000	8.0	0.47
15,000	9.0	0.47
15,500	3.8	0.70
20,000	8.0	0.24
20,000	9.0	0.24
20,400	3.8	0.43

The ratio of the surface temperature T_0 to the effective temperature T_e is definitely known for the gray atmosphere and is equal to $(1/\sqrt{3/4})^{1/4}$. For the case of non-gray atmosphere, the exact relation between T_0 and T_e is not known. However, it is concluded that T_0/T_e for non-gray case is less than $(1/\sqrt{3/4})^{1/4}$ (28). For our models, we used the gray temperature law, and there is no firm assurance that it would be a good approximation for the non-gray case. In the outer layer, the gray tem-

perature law is not a good approximation at all. The surface temperature of the non-gray atmosphere is lower than that of the gray atmosphere with the same effective temperature. Hence it is rather natural that the temperature in the outer layer of our mpdels is higher than temperature for real atmospheres. Therefore the absorption lines with pure absorption mechanism, computed with such a higher surface temperature, may become more shallow than it should be. We shall examine a correction to the temperature law of our models in the next section.

4. The revised models

The model atmosphere should be computed to obtain some knowledge about the structure of the real steller atmosphere. If one wishes to get a model which provides us with a satisfactory explanation of the continuous energy distribution in the stellar spectra, we have to compute a model atmosphere only valid in the layer from which the continuous flux emerges. On the other hand, if we want a model having a reasonable agreement with the observed ones in regard to the line spectra, which originate from the outer part of the atmosphere, it is necessary to have a model valid throughout the atmospheric layers where we can observe optically.

Our model atmospheres of white dwarf stars fail to predict satisfactorily the profile of Balmer lines. This is due to the applied gray temperature law. The discrepancy between computation and observation in H_γ profile is largest for model with $T_e=10{,}700\,^\circ$K. Here we shall examine models 181 and 191 in detail, and apply some corrections to these models.

We originally intend to obtain a model atmosphere in mechanical and radiative equilibrium. We got a model atmosphere integrating the differential equation which expresses mechanical equilibrium, with the use of temperature law in question. Hence the most simple method to test the model atmospheres is to check the constancy of the integrated net flux $F(\tau)$ throughout the optical depth τ. $F(\tau)$ can be easily computed by the following formula (cf. Eq. (14)):

$$F(\tau)=\int_0^\infty F_\nu(\tau)\,d\nu=\int_0^\infty \Phi_{\tau_\nu}(\tau)\left\{B_\nu(t_\nu)\right\}d\nu\,. \tag{29}$$

$F(\tau)$ for the models 181 and 191 are shown in Fig. 6. As expected, the deviation $\Delta F(\tau)$ from the mean value of flux, $\bar{F}$, is large in the outermost layers. This feature is common for model computed with the Rosseland mean opacity. As noted at the end of the previous section, in the outer layer of the atmosphere, the surface temperature of the gray atmosphere is too high. Furthermore, so far as the flux mean is concerned, the Rosseland mean is correct only in deep

layer (cf. Unsöld (**22**)), and hence the connection between non-gray and gray atmosphere which is kept by the mean opacity, becomes unreliable in the outer layer.

Here we will try to correct the temperature distribution in our model to obtain a better model in the outer layer of the atmosphere.

The methods to obtain a model atmosphere with constant net flux are divided roughly into two types; one is a rather analytical type, while the other is a numerical one. The former method is based on the iterational procedure using the fact that in radiative equilibrium the mean value of mean intensity weighted by the absorption coefficient is equal to that of source function and the so-called "*K-integral*" in radiative transfer problem holds. The mathematical expressions

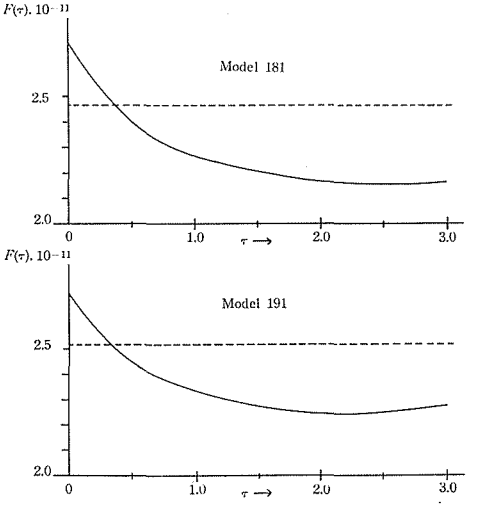

Fig. 6. $F(\tau)$ for the models with T_e=10,700°K.

equivalent to these statements are used as the fundamental equations in the iterative process. Such methods, named as "*Λ-Iteration*" or "*Strom-Iteration*", have been applied by Pecker (**36**) and by Hunger (**37**).

Although mathematically elegant, these essentially include integrations and/or differentiations, which should be completed by several numerical procedure. Hence there arises inevitable ambiguities in numerical values, such as originated from the rounding errors.

The second method, which aims to treat the problem in fully numerical manner, was proposed originally by Kourganoff (**21**). The problem to obtain a non-gray temperature distribution is in itself reduced to an integral equation. One approximates the solution of this integral equation by a finite series of

functions, and obtains equations for the coefficient of this series to minimize the errors in this approximation.

On similar lines, there is a more simple method (cf. Swihart (38)). As we have a model in the first approximation, and have the deviation of net flux $\Delta F(\tau)$ from a definite value, F, that is the total flux, either corresponding to the initially assumed effective temperature or defined as $\int_0^\tau \left\{\Delta F(\tau)\right\}^2 d\tau / \int_0^\tau d\tau$ becomes minimum, so as to get rapid convergence. Then we can seek a correction ΔB in the source function, to reduce this ΔF to zero. More strictly, we approximate ΔF by a linear combination of some functions, whose Φ-transformations are known, as:

$$\Delta F(\tau) = \sum_i A_i \Phi_\tau \left\{ f_i(t) \right\}, \tag{30}$$

and the correction ΔB in B is calculated by

$$\Delta B(\tau) = \sum_i A_i f_i(\tau) . \tag{31}$$

As is easily seen, the choice of the function $f_i(\tau)$ has serious effects on the final results. Since this method is entirely based on the computed $F(\tau)$, i. e., the net flux of continuous radiation, we should always remember that the correction ΔB obtained is referred to the continuous radiation, and here we have nothing to do in the outer layers to include the effect due to the line absorptions. Furthermore, the Φ-transformation, the weighted integral of source function over whole τ-space, is usually evaluated by 2- or 3-point Gauss' numerical integration and any correction in the source function at the outermost layer has no effect in this integration. Numerically, this method does not give sufficient corrections in the outermost layers of model atmosphere.

Here we will correct the model 191 to get a model with constant net flux. As is seen in Fig. 6, $F(\tau)$ of model 181 is entirely similar to that of model 191, hence it is sufficient to correct only the latter model, and the results obtained may also be applied to the former. The function ΔF, shown in Fig. 6, is approximated with the use of the Eq. (30), where we take following four functions as $f_i(\tau)$'s,

$$1, \tau, \exp\left[-\frac{1}{2}\tau\right], \quad \text{and} \quad E_2(\tau) . \tag{32}$$

The factor 1/2 in the exponential function is so chosen that the Φ-transform of this function may have similar behaviour to the $\Delta F(\tau)$ shown in Fig. 6.

If we have $\Delta B(\tau)$, we can easily obtain the correction $\Delta T(\tau)$ in the temperature distribution law. The revised temperature, $T_2(\tau)$, is then given by

$$T_2(\tau) = T_1(\tau) + \Delta T(\tau) . \tag{33}$$

$T_2(\tau)$ for this model is compared with $T_1(\tau)$ in Fig. 7. As expected, the surface temperature is much reduced. This means that the net flux $F(\tau)$ computed with the first approximation gives higher value in the surface region, that is, the outward flux in these layers is greater compared with this inward flux.

With this revised temperature distribution, we follow the same procedure as described in § 2. The same revised temperature law is applied to the model

Table 9-1. The revised model atmosphere.
Model 192; T_e=10,700°K, $\log g$=9.0.

τ	θ	T °K	$\log P_g$	$\log P_e$	$\log \kappa$	$\log y_H$	$\log y_{He}$
0.001	0.652	7.73(3)	5.520	2.930	0.638	$\bar{1}$.999	0.000
2	652	7.73	727	3.040	739	999	
5	651	7.75	6.000	190	867	999	
0.01	648	7.77	206	311	957	999	
2	643	7.84	411	454	1.070	0.000	
3	639	7.89	525	547	151	000	
4	634	7.95	603	624	216	000	
6	625	8.07	707	745	316	000	
8	616	8.19	776	847	394	000	
0.1	608	8.30	828	935	456	000	
14	593	8.50	901	4.088	566	$\bar{1}$.999	
2	574	8.78	971	267	692	999	
3	549	9.19	7.043	494	849	999	
4	528	9.54	090	671	974	998	
5	512	9.85	122	815	2.071	998	
6	498	1.01(4)	147	936	156	997	
8	475	1.06	182	5.129	293	996	
1.0	457	1.10	207	285	398	994	
1.4	429	1.17	251	519	569	991	
2.0	400	1.26	273	767	736	984	
3.0	367	1.37	305	6.039	943	971	
4.0	345	1.46	325	217	3.093	955	
5.0	328	1.54	340	344	182	938	
6.0	315	1.60	352	447	260	919	
8.0	295	1.71	370	597	354	879	
10.0	290	1.80	385	702	416	836	
14.0	258	1.95	410	838	481	745	
20.0	237	2.13	440	961	536	610	

with smaller surface gravity. In Table 9, the structure of these models are given.

We also computed the net flux $F(\tau)$ (Fig. 8). We find that the constancy of $F(\tau)$ is remarkably improved. However, as mentioned above, the surface temperature could not be determined exactly with this method. Any temperature law at small optical depth may predict similar constancy of $F(\tau)$. Hence, to define the temperature in outermost layers, we must use the features of absorption lines.

Table 9·2. The revised model atmosphere.
Model 182; T_e=10,7000°K, $\log g$=8.0

τ	θ	T °K	$\log P_g$	$\log P_e$	$\log \kappa$	$\log y_H$	$\log y_{He}$
0.001	0.652	7.73(3)	4.800	2.561	0.342	$\bar{1}$.977	0.000
2	652	7.73	5.017	676	428	998	
3	651	7.75	303	833	549	998	
0.01	648	7.77	509	956	666	999	
2	643	7.84	707	3.098	788	999	
3	639	7.89	819	190	863	999	
4	634	7.95	896	266	922	999	
6	625	8.07	6.002	387	1.011	999	
8	616	8.19	072	491	096	999	
0.1	608	8.30	124	579	165	999	
14	593	8.50	196	727	278	998	
2	574	8.78	265	906	412	998	
4	549	9.19	334	4.133	586	997	
3	528	9.54	377	310	721	996	
5	512	9.85	407	451	829	995	
6	498	1.01(4)	429	571	920	993	
8	475	1.06	460	762	2.074	990	
1.0	457	1.10	482	912	196	986	
1.4	429	1.17	510	5.140	379	978	
2.0	400	1.26	537	378	573	962	
3.0	367	1.37	563	628	776	929	
4.0	345	1.46	579	791	903	890	
5.0	328	1.54	593	902	977	846	
6.0	315	1.60	603	987	3.033	798	
8.0	295	1.71	622	6.090	089	692	
10.0	280	1.80	638	161	101	586	
14.0	258	1.95	669	255	092	391	
20.0	237	2.13	713	336	061	146	

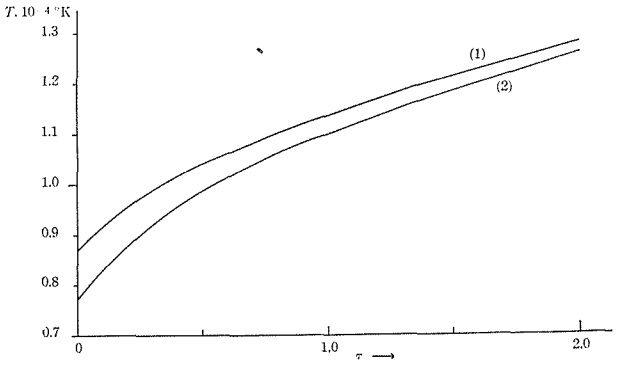

Fig. 7. $T(\tau)$.
(1); Initial $T(\tau)$. (2); Revised $T(\tau)$.

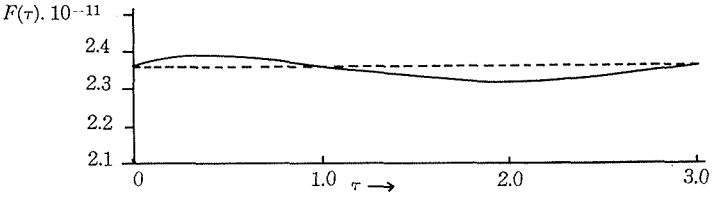

Fig. 8. $F(\tau)$ for revised model.

The emergent flux $F_\nu(0)$ for our revised models is given in Table 10, and shown in Fig. 9. The contours of Balmer lines are computed quite in the same way as in the initial models. The color indices are found that they slightly

Table 10. The emergent flux of the revised model.

ν	Model		ν	Model	
	192	*182*		*192*	*182*
3.288_- (15)	0.24(−4)	0.26(−4)	4.938	1.51	1.56
2.932	28	30	4.612	1.45	1.50
2.576	34	36	4.133	1.35	1.38
2.220	43	42	3.653_+	1.21	1.24
1.865	55	53			
1.509	74	69	3.653_-	1.25	1.28
1.153	1.00	92	2.854	0.98	1.01
9.875(14)	1.13	1.03	2.055	66	0.66
8.220_+	1.25	1.12	T_e* °K	1.07(4)	1.07(4)
8.220_-	1.68	1.87	*U-B*	−0.82	−0.64
6.742	1.67	1.81	*B-V*	+0.12	+0.08
5.263	1.56	1.63	*U-V*	−0.70	−0.56

differ from the initial models (see Table 10). However, the difference is not so large that the temperature scale should be changed.

In Figs. 10·1 and 10·2, we compare the profiles of Balmer lines of model 182 with observed ones. We see that the agreement is greatly improved for this model. We may certainly conclude that 40 Bri B and 73° 8031 have effective temperature around 10^4 °K. Comparing their $U-V$ color, -0.67 for 40 Bri B and -0.65 for 73° 8031, with -0.56 for model 182, we have a slightly higher effective temperature than $T_e=10^4$ °K, for these stars.

The $U-V$ color for W 485 is -0.56. We give a comparison of model 182 with this star in Fig. 10·3. This star is also well represented by model 182.

Here we have discussed only model 182. The line profiles of model 192 are slightly shallower than those of model 182. Hence, the observed profiles are

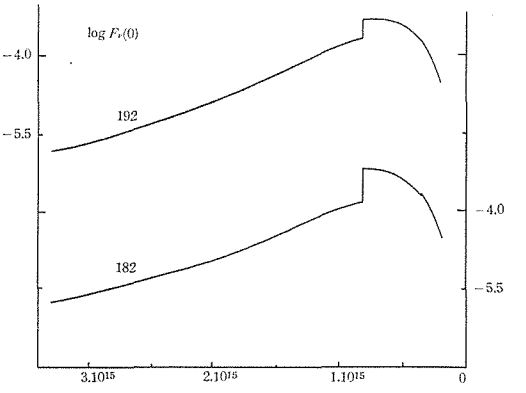

Fig. 9. Emergent flux for revised models.

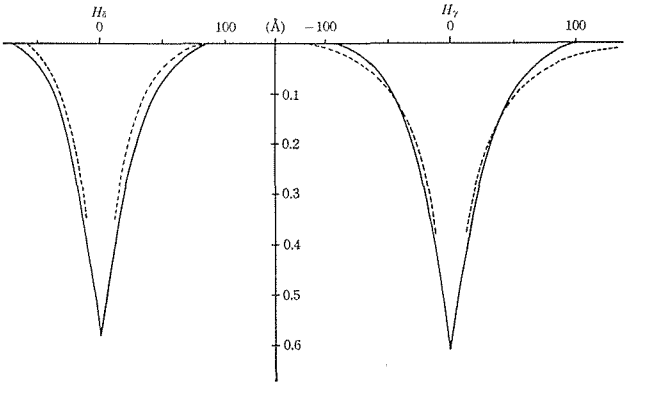

Fig. 10·1. Comparison with 40 Eri *B*.
--- Model 182.

said also to be predicted with model 192. However, the color indices prefer model 182 to model 192.

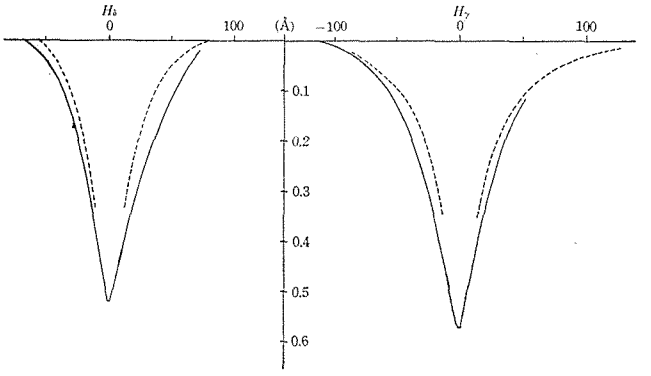

Fig. 10·2. Comparison with 73° 8031.
– – – Model 182.

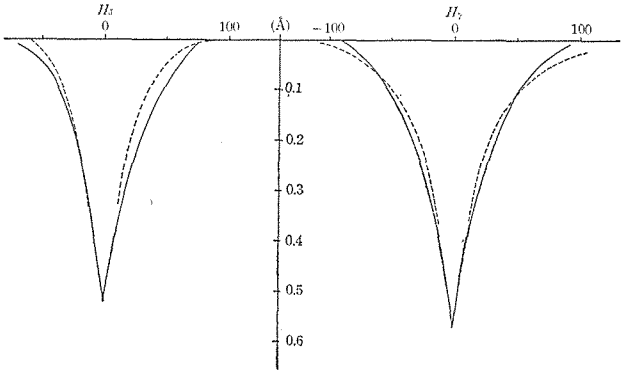

Fig. 10·3. Comparison with W 495.
– – – Model 182.

5. Conclusion

As already mentioned, there are some evidences that white dwarfs are deficient in hydrogen. The so-called DC type star has a similar $U-V$ color to DA type, and if this color is used to calibrate the temperature scale, anomaly of chemical composition should be necessarily taken into account.

On the other hand, it is found that there are white dwarfs with enormously large hydrogen absorption lines in their spectra. The aim of this paper is to explain such large hydrogen lines with the use of hydrogen rich model atmosphere,

We constructed a series of model atmospheres with gray temperature distribution law. We obtained a relationship between color indices and effective temperature based on hydrogen rich model atmosphere. With this relation, the effective temperature of the DA type white dwarfs are calibrated (see Fig. 3). If we consider the distribution of DA type star against the $U-V$ color indices, we see that majority of DA type stars has effective temperature around 10^4 °K or lower. Then it is necessary to extend the series of models to the lower effective temperature to establish temperature-color relation for wider range of DA type stars.

We computed Balmer line profiles and compared them with observation. It is found that the models with gray temperature law are unsatisfactory for this purpose. The computed equivalent widths of the Balmer line are smaller than the observed ones and this discrepancy is pronounced in lower temperature models. We sought the reason of this discrepancy in the incorrect temperature distribution in outer layer of our model atmosphere. Correcting the temperature law in outer layer of models we got revised model atmospheres in which the net flux of radiation is sensibly constant. With these corrected models we could predict the deep hydrogen absorption lines in lower temperature white dwarfs.

However, we cannot put much reliance on this success of our method. The correction applied to the models is to reduce the deviation ΔF in total flux from the constant net flux F. Here, the net flux $F(\tau)$ is considered as the total flux composed of the continuum and excluding the existance of line absorption. The work is fully numerical, and the ϕ-integration is done with the Gauss numerical quadrature. As far as the division points and weights based on this method are used, source function at the optical depth $\tau \lesssim 0.1$ has little influence on the resultant $F(\tau)$. Hence any temperature distribution in $\tau \lesssim 0.1$ yields an identical value $F(\tau)$. The correction, applied to temperature law in §4, is trustworthy in deep layer, such as $\tau \gtrsim 0.1$ Furthermore, there is another question concerning the function $f_i(\tau)$ in the expansion of source function (cf. Eq. (30)). This choice is fully arbitrary, and there are no *a priori* criteria on this point.

The spectra of DA type white dwarfs show the large Balmer absorption lines suggest that the radiation field at the outermost layer must be affected considerably by these line absorptions. Such blanketing effect will reduce the surface temperature. In this paper we did not take this effect into account. Nevertheless, we could predict correctly the Balmer line profiles. As the temperature at the outermost layer cannot be specified by the correction, the derived temperature in §4 might fortunately represent temperature-drop at the surface, which would occur, if the line blanketing were considered. In this sense, the choice

of base function would have an important role.

For the purpose of comparing theoretical models with observations, we used only the color indices and Balmer line profiles. To study the DA type white dwarfs, it is the very handicap that these stars do not show any line spectra other than Balmer lines. Hence we cannot take other criteria than those in this paper to check the model atmosphere. As for the model atmosphere there are some degrees of freedom, that is, chemical composition, effective temperature and surface gravity. Further, we do not know the precise temperature distribution in non-gray atmosphere. Hence, for the purpose to explain the atmosphere of white dwarf stars, we have nothing to say with a few models. We may treat problem in statistical manner. We should construct more series of models for white dwarfs with various parameters such as difference in chemical composition, and examine whether the consistent series of models can be obtained which predict well observed color and Balmer line profiles. In regard to these points, it is interesting to deal with the low temperature models where the ratio of hydrogen to heavy element has great importance as the electron source which influences the opacity of the atmosphere.

Acknowledgments

The author would like to express his cordial thanks to Prof. S. Miyamoto who suggested the present problem and encouraged him continually. The author's thanks are also due to Prof. S. Ueno for his guidance and invaluable suggestion and further, to Dr. J. Jugaku, who kindly suggested him to compute the Balmer line profile with the use of Kolb's theory and to Dr. S. Saito for his suggestion and helpfull discussion.

REFERENCES

1. B. Strömgren: Publ. Medd. Kobenhavn Obs., No. 127 (1940).
2. L. H. Aller: *Handbuch der Physik* Bd. 51 (1958), 324.
3. C. de Jager and L. Neven: Ann. Obs. Roy. Belgique, VIII, Fasc. **1** (1957).
4. S. Miyamoto: Mem. Astrophys., **1** (1946), 17.
5. E. Schatzman: Publ. Kobenhavn Obs., No. 149 (1949).
6. R. Grenchik: Ap. J., **62** (1957), 16.
7. P. Couteau: Ann. d'Ap. Suppl. No. 3 (1957).
8. S. Chandrasekhar: *An Introduction to the Study of Stellar Structure*, (Chicago, 1939).
9. G. P. Kuiper: *Les Naines Blanches: Découverte, Observations, Conditions de Surface. Les Novae et les Naines Blanches III*, 212, (Paris, 1941).
10. B. T. Lynds: Ap. J., **125** (1957), 719.
11. J. L. Greenstein: *Handbuch der Physik*, Bd. 50 (1958), 161.
12. W. J. Luyten: Ap. J., **116** (1952), 283.
13. J. L. Greenstein: *Stellar Atmosphere*, (Chicago, 1960) Chapt. 19.

14. V. WEIDEMANN: Ap. J., **131** (1960), 638.
15. S. SAITO: Contr. Inst. Astrophys. Kyoto, No. 48 (1954).
16. S. SAITO: *ibid.*, No. 69 (1956).
17. S. SAITO and A. UESUGI: Contr. Inst. Astrophys. and Kwansan Obs., No. 78 (1959).
18. S. UENO: Contr. Inst. Astrophys. Kyoto, No. 42 (1954).
19. A. UNSÖLD: *Physik der Sternatmosphären* (2 Aufl., Berlin, 1955).
20. C. MARK: Phys. Rev., **72** (1947), 558.
21. V. KOURGANOFF: *Basic Method in Transfer Problem* (Oxford, 1952).
22. A. UNSÖLD: Zs. f. Ap., **25** (1948), 340.
23. R. MICHARD: Ann. d'Ap., **12** (1949), 291.
24. P. TEN BRUGGENCATE: Veröff, Univ.-Stermwarte, Göttingen, Nr. 96 (1950).
25. S. SAITO: Contr. Inst. Astrophys. and Kwasan Obs. No. 79 (1959).
26. D. LABS: Zs. f. Ap., **27** (1950), 153.
27. S. UENO, S. SAITO and J. JUGAKU: Contr. Inst. Astrophys. Kyoto, No. 43 (1954).
28. G. MÜNCH: Ap. J., **104** (1946), 87.
29. H. M. JOHNSON and W. W. MORGAN: Ap. J., **114** (1951), 522.
30. E. PETTIT: Ap. J., **91** (1940), 159.
31. H. M. JOHNSON and W. W. MORGAN: Ap. J., **117** (1953), 313.
32. L. H. ALLER and J. JUGAKU: Ap. J., **128** (1958), 616.
33. H. R. GRIEM, A. C. KOLB and K. Y. SHEN: Phys. Rev., **116** (1959), 4.
34. L. H. ALLER and J. JUGAKU: Ap. J., **130** (1959), 469.
35. H. R. GRIEM: Ap. J., **132** (1960), 883.
36. J. C. PECKER: Ann. d'Ap., **13** (1950), 433.
37. K. HUNGER: Zs. f. Ap., **36** (1955), 42.
38. T. L. SWIHART: Ap. J., **123** (1956), 143.